



A new approach in evaluation impacts of teleconnection indices on temperature and precipitation in Iran

Mohammad Ahmadi¹ · Mohammad Kamangar² · Saadoun Salimi³ · Seyed Asaad Hosseini⁴ · Yeganeh Khamoushian⁵ · Sousan Heidari⁶ · Gholamreza Maghami Moghim⁷ · Vahideh Saeidi⁸ · Ismaeil Bakhshi² · Zahra Yarmoradi⁵

Received: 22 February 2022 / Accepted: 1 July 2022 / Published online: 18 July 2022
© The Author(s), under exclusive licence to Springer-Verlag GmbH Austria, part of Springer Nature 2022

Abstract

In many parts of the world, teleconnection patterns are one of the climate phenomena that significantly change the causative climate anomalies, especially temperature and precipitation. Thus, statistical analysis and modeling of their effects are of great importance in order to understand the fluctuations and climate variability in a region. In this study, 52 teleconnection indices were utilized to perform statistical analysis and conceptual modeling as well as simulation of temperature and precipitation fluctuations in Iran. For this purpose, temperature and precipitation data of 36 synoptic stations in Iran and 52 teleconnection indices for the period 1951–2019 were used. For the analysis, the relevant data were classified into four groups of global (GLB), regional (RGN), El Niño–Southern Oscillation (ENSO), and all indices (ALL). Then, the correlation of the aforementioned indices with temperature and precipitation was calculated using the teleconnectional–statistical model (TSM). Afterward, 5 years with the highest correlation coefficient was selected and considered as the forecasting parameters. The results revealed that the local temperature forecasting using RGN indices and the precipitation forecasting using GLB and ALL indices were more accurate than those using other indices. Our findings highlighted the prominent role of the indices with broader geographical regions that mainly were evolved across the oceans. Moreover, the effect of ENSO teleconnection on Iran climate was explained by the dynamic mechanism of the atmospheric bridge. Comparing TSM outputs and the Climate Forecast System Version 2 (CFSV2), TSM outperformed CFSV2 in the conducting experiment. Overall, the findings of this study emphasized on the existence of coincided synergy in the fluctuation or trend within almost all indices and atmospheric parameters, and most of the fluctuations in the indices occurred simultaneously or right after the ENSO events, including specific super El Niño in 1997–1998 (turning point). Also, the dramatic effect of sunspots on the average temperature of Iran is shown in inverse harmony, which is not easily revealed by correlation analysis. Also, the influence of global warming and especially synchronization with El Niño event on climatic change was briefly discussed in the Middle East. In this work, for the first time in the Middle East, physical mechanisms of how linkages affect Iran’s climate and rainfall were proposed in a synoptic conceptual model.

✉ Seyed Asaad Hosseini
Hosseini.asad8@gmail.com

¹ Kermanshah Regional Meteorological Office, Kermanshah, Iran

² Department of Geography, Zanzan University, Zanzan, Iran

³ Department of Geography, Kharazmi University, Tehran, Iran

⁴ Kurdistan Province Meteorological Office, Sanandaj, Iran

⁵ Department of Geography, Lorestan University, Lorestan, Iran

⁶ Department of Geography, University of Tehran, Tehran, Iran

⁷ Department of Geomorphology, University of Damghan, Damghan, Iran

⁸ Department of GIS & RS, University of Tehran, Tehran, Iran

1 Introduction

The climate of each region is affected by global and regional atmospheric indices, patterns, and forces. Climate patterns and indices are the criteria by which the temporal fluctuations of intensity and spatial variations of atmospheric circulation patterns are measured in one region and compared with other regions and can be used to detect climate change and predict atmospheric behavior (Ahmadi et al. 2019). Hence, the significant correlations between temporal changes of two patterns or atmospheric circulation systems within two long-distance regions are called teleconnection (Bridgman and Oliver 2006). Teleconnection is a way to condense atmospheric patterns with a description regarding the processes of Earth-atmosphere momentum exchange (Schwing et al. 2009). This phenomenon is generally an analysis of the relationship between low-frequency fluctuations of atmospheric circulation, precipitation, and the tropical and subtropical temperatures with the tropics, especially in relation to the El Niño–Southern Oscillation (ENSO) phenomenon (Ding and Wang 2005). In other words, the teleconnection is the relationship between atmospheric circulation changes in the Pacific Ocean and the North America regions with the surface temperature of the North Pacific (Klein et al. 1999). In fact, one of the climate phenomena, the change of which causes great anomalies of climate, particularly on temperature and precipitation patterns in many parts of the world, is teleconnection, and it is very important to reveal the relationship between them and climatic parameters for a better understanding of oscillation and climate variability in every area (Goudarzi et al. 2017). Various studies were conducted to predict climate parameters using such indices and similar statistical methods; Rezaie and Memarian (2014) investigated the efficiency of coactive neuro-fuzzy inference system (CANFIS) in predicting drought in Birjand, Iran, by combining large-scale climate signals with precipitation and Standardized Precipitation Index (SPI) (drought index). Among their models, a model with combination of input parameters of NINO1 + 2 models (with a 5-month delay and no delay), monthly precipitation, and NINO3 (with a 6-month delay) with a correlation coefficient of 0.9 (between observed and predicted values) represented as the most suitable model for drought prediction in the region using CANFIS network. Yari et al. (2014) studied forecasting the precipitation in Saghez, Iran, using artificial neural network (ANN) and emphasized on the high ability and robustness of ANN for monthly prediction.

Honar et al. (2016) studied droughts in Sistan and Baluchestan using Markov chain and SPI to estimate appropriate cropping patterns. Their studies measured the

probability of equilibrium of wet, dry, and normal periods by 2.7%, 35.14%, and 62.16%, respectively, in Zabol station. They categorized the most of the regions as normal climate conditions, while the probability of dry year was thirteen times more than that of wet year. Mohammadpour Penchah and Taghizadeh (2016) explored the trend of monthly temperature changes in Bandar Abbas station, Iran, using ARIMA models and the Box–Jenkins approach. They highlighted the successful use of Box–Jenkins in the prediction of minimum and maximum temperatures.

In examining the summer monsoon changes of the Arabian Peninsula with the ENSO and dipole teleconnection patterns of the Indian Ocean, Charabi (2009) showed that the summer monsoon changes were highly correlated with the circulating and convective currents in the equatorial part of the Indian Ocean and ENSO. Over the last four decades, the influence of the ENSO and dipole of Indian Ocean fluctuation on the summer monsoon of Southern Oman has mainly increased. Shifteh et al. (2012) studied the spatial temporal trend and precipitation changes, in Iran. They reported that Iran mostly experienced a negative annual precipitation trend and that trend was greater in spring and winter than other seasons. Besides, the maximum decrease in winter precipitation was observed on the northern half of Iran as the prevalent season of the year. Dayan et al. (2016) worked on the preconditioning of heavy precipitation in the Mediterranean Basin and showed that moisture convergence played a significant role in the occurrence of heavy precipitation. The authors concluded that the most significant correlation between precipitation and the northern fluctuation index occurred in the northwest of the basin (Iberia). Gerlitz et al. (2016) investigated the predictability of the Southwest and Central Asia precipitations using water surface temperature data and ENSO. Ahmadi et al. (2019) studied the teleconnection modeling in connection with precipitation, and their findings emphasized on the direct role of ENSO on precipitation in Iran. Darand and Pazhoh (2019) considered the significant role of southern latitude thermal system and high-latitude dynamics system in precipitation and occurrence of wet periods in Iran. According to their findings, the main synoptic patterns for the occurrence of pervasive and durable precipitation were Saudi Arabia low-pressure trough penetration at sea level and Arabian subtropical high-pressure and deep trough penetration from high latitudes in the middle levels of the troposphere.

In South Asia, the study of temperature and heavy precipitation by Naveendrakumar et al. (2019) indicated an increase in severe temperatures in most countries of the region, which had also increased the severity of drought and flood events. Atif et al. (2020) analyzed the heavy precipitation of the Saudi Arabia's wet season in relation to teleconnection patterns and concluded that the occurrence of heavy precipitation in that region had a great connection

with ENSO. Helali et al. (2020) investigate the effect of teleconnection phenomena on autumn precipitation in Iran's watersheds. Result showed that the ENSO family indices have the most significant correlation with most studied basins, especially the peripheral and western basins of Iran.

In this study, we aim to evaluate the feasibility of simulation and monthly forecasting of temperature and precipitation in Iran, especially in terms of teleconnection patterns and their applicability by various sectors. Therefore, the objectives are to analyze the teleconnection indices and model the effect of ENSO forcing on Iran climate.

2 Data and methodology

The study area is within Iran borders with dominant arid and semi-arid climate. The study area is located in latitudinal coordinates between 25° and 39° N and longitudinal coordinates between 44° and 64° E with the area of 1,648,000 km² in the Middle East. The average annual precipitation of Iran is recorded by one-third of the average precipitation in the world (Salimi et al. 2018). Iran, as one of the most mountainous countries in the world, is dominated by rugged mountain chains such as the Zagros and Alborz in the west and north, respectively, separating different basins or plateaus. The geographical location of this mountain range has created large deserts (i.e., Lut and Kavir deserts) significantly affecting the Iran's climate (Shiravand and Hosseini 2020). The climate of the northern part of Iran is Mediterranean and humid; however, most of the Iran exhibits arid or semi-arid climate (Helali et al. 2022).

The geographical location of the study area and the meteorological stations are shown in Fig. 1a, and the geographical characteristics of meteorological stations are presented in Table 1. For the present study, monthly data of 52 teleconnection indices from valid global databases including NOAA, the Bureau of Meteorology (BOM), Japan Meteorological Agency (JMA), and KNMI Climate Explorer (climexp.knmi.nl) databases, and temperature and precipitation data of 36 main meteorological stations were acquired from Iran Meteorological Organization (IRIMO) in the period 1951–2019.

Regarding the inadequacy and homogeneity of stations in the central regions of Iran, most of these areas are uninhabited and there are no valid stations. On the other hand, simulated and interpolated data of models or satellites are reflected in reanalysis maps. They have many errors. Also, many stations in Iran have started recording statistics after 1985, and the accuracy of predictions and model training depends on long-term statistics with a variety of wet–dry and cold–hot periods. Therefore, the limited number of available stations has inevitably been used. To ensure the adequacy of the stations, instead of comparing with the

erroneous data of the reanalysis, the 2 months representing the cold and warm seasons of the year (January/February) were compared with the actual rainfall statistics of 145 stations in the country, which are close to 4 times the main stations. (The statistical base of this group is 145 stations, which overlap with a set of 36 stations, after 1985.) Long-term precipitation maps in these two representative months show acceptable consistency in the modeling of the present study; this shows that, although the stations used in this study are 1/4 of the sample stations, there is no significant change in the pattern and spatial zoning of precipitation. This reaffirms that classical and frontal precipitation systems operate on a synoptic scale, and that the lack of proper station coverage is important only in torrential and convective precipitation. Based on the rainfall maps of 36 and 145 stations, it is very important to note that despite the threefold import of stations, the central regions of Iran still face a lack of adequate coverage. In general, as mentioned before, most of the central and eastern parts of the country have more or less the same rainfall. Using the spatial correlation analysis method, the correlation value between the precipitation map of January 36 stations and 145 stations was 0.891 and the correlation value between the July precipitation map of 36 stations and 145 stations was 0.821. These high correlations indicate the relatively good representation of 36 stations in most parts of Iran. The reanalysis output is also given for comparison. The important point in the output reanalysis of the month of January is that it is a rainy core in the central regions of Iran, which is completely wrong. For the month of July, it has not been able to simulate the summer rains in southeastern Iran due to the influence of eastern waves and expansion of Southwest Asia monsoon (Fig. 1b–e).

Next, the Pearson correlation coefficient matrix of the teleconnection indices with temperature and precipitation of the main meteorological stations was formed using Eq. (1).

$$r_{x,y} = \frac{\sum(x_i - \bar{x})(y_i - \bar{y})}{\sqrt{(\sum(x_i - \bar{x})^2)(\sum(y_i - \bar{y})^2)}} \quad (1)$$

where x and y are independent and dependent measures, respectively (the two sets of data), and the obtained r value is between -1 and $+1$. The perfect positive and negative correlations within the variables are defined by the positive and negative values of 1, as well (Asakareh and Ashrafi 2012).

In this study, map interpolation was performed using ArcGIS software and the statistical analysis and chart were performed and generated by SPSS software and Microsoft Office Excel.

Root-mean-square error (RMSE) was calculated for the dataset by Eq. (2).

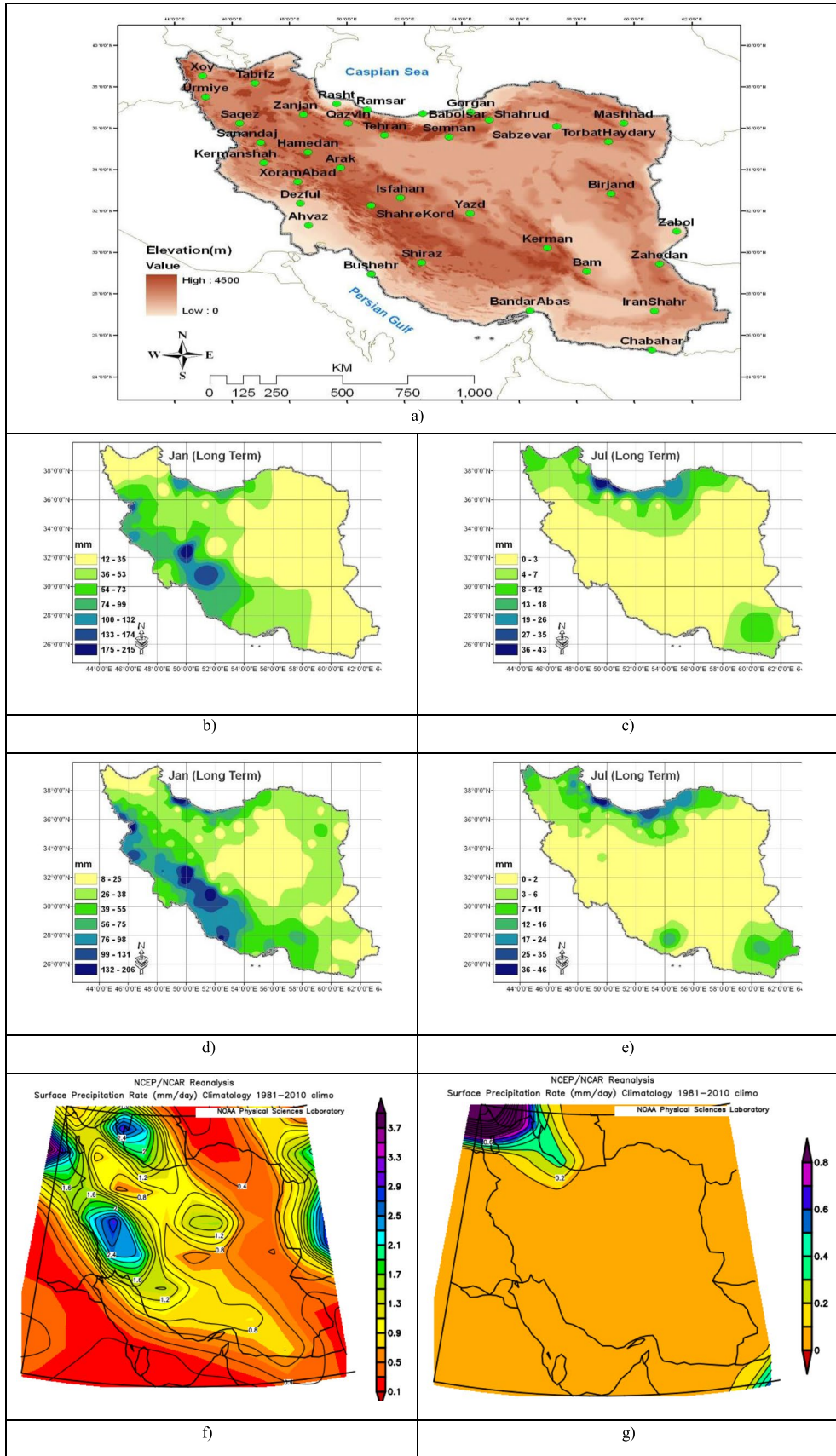


Fig. 1 **a** The topographical map of the study area and location of meteorological stations. **b–g** The long-term monthly precipitations. **b** January average rainfall using 36 stations. **c** July average rainfall using 36 stations. **d** July average rainfall using 145 stations. **e** July average rainfall using 145 stations. **f** January average rainfall using reanalysis environment (the rain rate must be multiplied by 31). **g** July average rainfall using reanalysis environment (the rain rate must be multiplied by 31)

$$\text{RMSE} = \sqrt{1/N \sum_{i=1}^n (F - O)^2} \quad (2)$$

where N , F , and O are the number of test, forecasted value, and observation (temperature), respectively (Asakareh and Ashrafi 2012).

The methodology for this research was based on the conceptual modeling and factor analysis. The most significant indices of teleconnection were selected from all indices and were consequently classified into four groups (Table 2) of global indices with 20 indices (GLB), ENSO with 12 indices (ENSO), regional indices with 20 indices (RGN), and a combination of all indices (ALL: GLB, ENSO, and RGN). Finally, their correlation coefficients with the temperature and precipitation were calculated by teleconnectional–statistical model (TSM¹).

Here, for the first time in Iran region, some common and well-known teleconnection indices together with some temperature and pressure parameters that were less affected by these indices were used as complementary data to calculate the correlation matrix. In fact, the invisible force field around the Earth and other levels in Iran climate were more directly and effectively introduced to the statistical models by these complementary indices. Then, the averages of four main groups (ALL, GLB, ENSO, and RGN models) with the mean temperature and precipitation of each station were determined (in the order of 5 years) by applying an analog approach of the priority weight with the highest Pearson correlation coefficient as input for prediction and forecasting. It is based on the simple and synoptic assumption with the establishment of the same patterns as global and regional teleconnection which comparatively causes the similar behaviors of atmospheric systems, near to the years extracted in the statistical period in the present study. However, it can be done and interpreted by the assumption of stable (static) geophysical and cosmic conditions within the next few months in the forecast period. Due to the complexity and non-linearity of atmospheric–oceanic circulation and the simplifications of linear models, it should be cautiously investigated by considering the standard deviation and calibration of the temperature.

The reasons for classification into four groups are as follows: Indices are classified according to the type (e.g., pressure indices such as North Atlantic Oscillation (NAO)) or temperature indices (e.g., SSTs and Niños) or wind/advection indices (e.g., Pacific East Wind indices) or their region. Mostly in this study, for a phenomenon like ENSO, the manual combination of geographical distribution, type, and principal component analysis (PCA) matrix was used (not shown). We tried to categorize some of the indices into more suitable group which did not fit in a specific geographical distribution or did not have a high factor loading. For example, the Pacific Decadal Oscillation (PDO) index had the most similarity with the ENSO family in terms of structure, type, and geographical location. Moreover, we had to include the IOD index in the type of global indices because it was related to Walker and ENSO circulation and Asian–African monsoon.

To predict monthly and seasonal temperatures and precipitation, the closer teleconnection index data (in terms of time) are used, and higher accuracies are achieved in the predictions. The presence of some conditions between the two warm events of ENSO was the reason to select the year 2017 for this study. The strong El Niño in 2014 and 2015, post-El Niño and moderate La Niña in 2016, and moderate El Niño in 2018 occurred, which could have created confusion in the results and exaggerate the degree of accuracy in the output for the mentioned classic patterns.

In addition, the accuracy evaluation of the models was not the focus of this research and it was only assessed in Fall 2017, then it was not feasible for the rest of the study. The objective was to introduce and measure the applicability of such simple but very practical approach. Although the solar indices are not seemingly categorized as teleconnection indices, they are the main source of all teleconnections according to the energy source and fuel supplier of the ocean–atmosphere super machine (Ahmadi et al. 2019). Owing to the extremely large datasets and heavy calculations, it was very challenging to study more cases. Therefore, the outputs were only compared with the Climate Forecast System Version 2 (CFSV2) model.

The purpose of classifying indices is to find the main assumptions and the separate role of each. Due to regional differences and some indices, this division is inevitable because of some indices being compressive, some temperature, some geopotential, some advection, and so on. In fact, classification is one of the most important first steps in science. As mentioned above, the indices studied in this study are different in terms of spatial, level, and type; therefore, their classification is very helpful in discovering the hidden connections, processes, and forces of feedback. Except for the three groups mentioned, all indicators are considered as a whole. On the other hand, the indices in the ENSO group are well known and are in the same group. Regional

¹ In fact, this model is a new analog prediction model.

Table 1 Geographical characteristics of meteorological stations

Row	Station	Latitude (N)	Longitude (E)	Height (m)	Annual precipitation (mm)	Average temperature (°C)
1	Arak	34.10	49.77	1708	331	13.8
2	Urmia	37.53	45.08	1316	332.1	11.3
3	Isfahan	32.67	51.87	1550	125.4	16.5
4	Ahvaz	31.33	48.67	23	235.9	26.3
5	Iran Shahr	27.20	60.70	591	113.3	27.6
6	Babolsar	36.72	52.65	-21	913.2	16.9
7	Bam	29.10	58.35	1067	56.1	23.0
8	Bandar Abbas	27.22	56.37	10	177.2	27.3
9	Bushehr	28.98	50.83	20	259.4	24.8
10	Birjand	32.87	59.20	1491	166.9	16.7
11	Tabriz	38.20	46.80	1361	279.4	12.3
12	Torbat Haydaryeh	35.38	59.10	1451	271.7	14.8
13	Tehran	35.68	51.32	1191	241	17.5
14	Chabahar	25.30	60.62	8	116.6	26.6
15	Xoram Abad	33.43	48.28	1148	507.8	17.3
16	Xoy	38.55	44.97	1103	295.6	12.7
17	Dezful	32.40	48.38	143	398.5	24.4
18	Ramsar	36.90	50.70	25	1194.5	16.2
19	Rasht	37.20	49.65	37	1355.1	16.2
20	Zabol	31.03	61.48	489	62.9	22.7
21	Zahedan	29.47	60.88	1370	77.6	18.8
22	Zanjan	36.68	48.48	1663	304.2	11.6
23	Sabzevar	36.10	57.30	978	194.3	17.7
24	Saghez	36.25	46.27	1523	489.9	12.1
25	Semnan	35.58	53.55	1131	141.8	18.4
26	Sanandaj	35.33	47.00	1373	455.4	14.3
27	Shahrud	36.42	54.95	1345	164	14.5
28	Shahre Kord	32.28	50.85	2049	333.5	12.2
29	Shiraz	29.53	52.60	1484	326.9	18.1
30	Qazvin	36.25	50.05	1279	320.7	14.4
31	Kerman	30.25	56.97	1754	137.5	17.1
32	Kermanshah	34.35	47.10	1319	455.5	14.8
33	Gorgan	36.80	54.31	13	579.6	17.8
34	Mashhad	36.27	59.63	999	255.4	14.4
35	Hamedan	34.87	48.65	1742	318.9	12.0
36	Yazd	31.90	54.28	1237	60.1	19.6

indices also directly affect the climate of the Middle East and Iran. Also, most of global forces (indices) generally act in planetary scale and energy sources, as the mother of energy means the great Sun. In fact, the global effects of the ENSO warm phase (El Niño) and other indices reach the Middle East through these intermediate indices and regional representatives. For example, the effect of ENSO on the phases of the NAO is such that it usually causes a tendency to its positive phase, and this phase usually coincides with the wetting of the region, because the positive phase of NAO further enhances cyclogenesis in the Eastern Mediterranean (Alemzadeh et al. 2013). However, in recent years, there

have been changes in precipitation patterns that may be due to changes in the number and amplitude of Rossby waves and the quasi-resonance amplification (QRA) mechanism.

One of the following is explained about how to calculate in the TSM: For example, Iran's precipitation forecast for the autumn of 2017 year is presented. First, the Pearson correlation was calculated between the teleconnection data for July, August, and September and the monthly precipitation in October, November, and December. Then, the average precipitation of each station in first 5 years with a higher correlation was taken as the prediction. The first year had more weight and effect than the following years, so their

Table 2 Teleconnection indices in the present study in three main groups (ENSO, GLB, RGN)

	Explanation and (the source)
(1) ENSO family indices	
MEI	Multivariate ENSO index (NOAA)
SOI	Southern Oscillation Index (NOAA)
POI	West–East Pacific Difference Index (NOAA)
SST34	Nino 3.4, anomaly of sea surface temperature almost in central Pacific Ocean (NOAA)
TNI	Temperature difference between the east and center of the tropical Pacific (NOAA)
EQTHMBs	The difference between the temperature of the center of the Pacific Ocean and the temperature of the high-pressure Humboldt Basin (NOAA)
WPsst	West Pacific SST anomalies (NOAA)
U200CP	Wind orbital index of 200 h on the Pacific Ocean (JMA)
U850WP	Trade winds of 850 hPa on the western Pacific (JMA)
U850CP	Trade winds of 850 hPa on the center Pacific (NOAA)
U850EP	Trade winds of 850 hPa on the eastern Pacific (JMA)
PDO	Pacific Decadal Oscillation (NOAA)
(2) Global (GLB) indices	
SFLUX	Sun flux energy (NOAA)
SSPOT	Sun spots (NOAA)
GTA	Global temperature anomaly (KNMI)
CO ₂	CO ₂ values, Hawaii (KNMI)
QBO	Quasi-Biennial Oscillation at 30 mb (NOAA)
AMO	Atlantic Multi-decadal Oscillation (NOAA)
TNATSAdf	North Atlantic temperature gradient from south (NOAA)
WHWP	Western Hemisphere Warm Pool (NOAA)
IOD	Indian Ocean Dipole (BOM)
IOBsst	Tropical Indian Ocean temperatures
PNA	Pacific North American (NOAA)
WP	West Pacific pattern (NOAA)
CINDCATLs	Temperature gradient of the center of the Indian Ocean from the center of the Atlantic Ocean (NOAA)
MDGs	South Indian Ocean SST Index (NOAA)
RMM12df	Madden–Julian Index deferential
PHASE	Madden–Julian Index phase
MJO2070df	Madden and Julian Oscillation difference between 20 and 70°
Ta500	Temperature anomalies at the 500 hPa level in the Northern Hemisphere (NOAA)
(3) Regional (RGN) indices	
NAO	North Atlantic oscillation (NOAA)
SCN	Scandinavian Index (NOAA)
EAWR	East Atlantic–West Russian (NOAA)
POL	Polar Index (NOAA)
U200IND	200 hPa zonal wind index over the Indian Ocean (JMA)
MEDS	Mediterranean average SST Index (NOAA)
EWMEDs (MTI)	Mediterranean zonal SST gradient index, Mediterranean Temperature Index (NOAA)
NINDs	North Indian Ocean SST Index (NOAA)
PRs	Persian Gulf SST Index (NOAA)
XZRs	The Caspian Sea SST Index
BLKs	The Black Sea SST Index (NOAA)
RDSs	The Red Sea SST Index (NOAA)
MNSNSDNLOW	Sudan–Indian SLP Gradient (NOAA)
Iran QFF	Iran's plateau mean pressure index, box 15 to 40° northern and 45 to 65° eastern (NOAA)

Databases from NOAA, BOM, JMA, and KNMI Climate Explorer databases.

SST sea surface temperature, SLP sea level pressure.

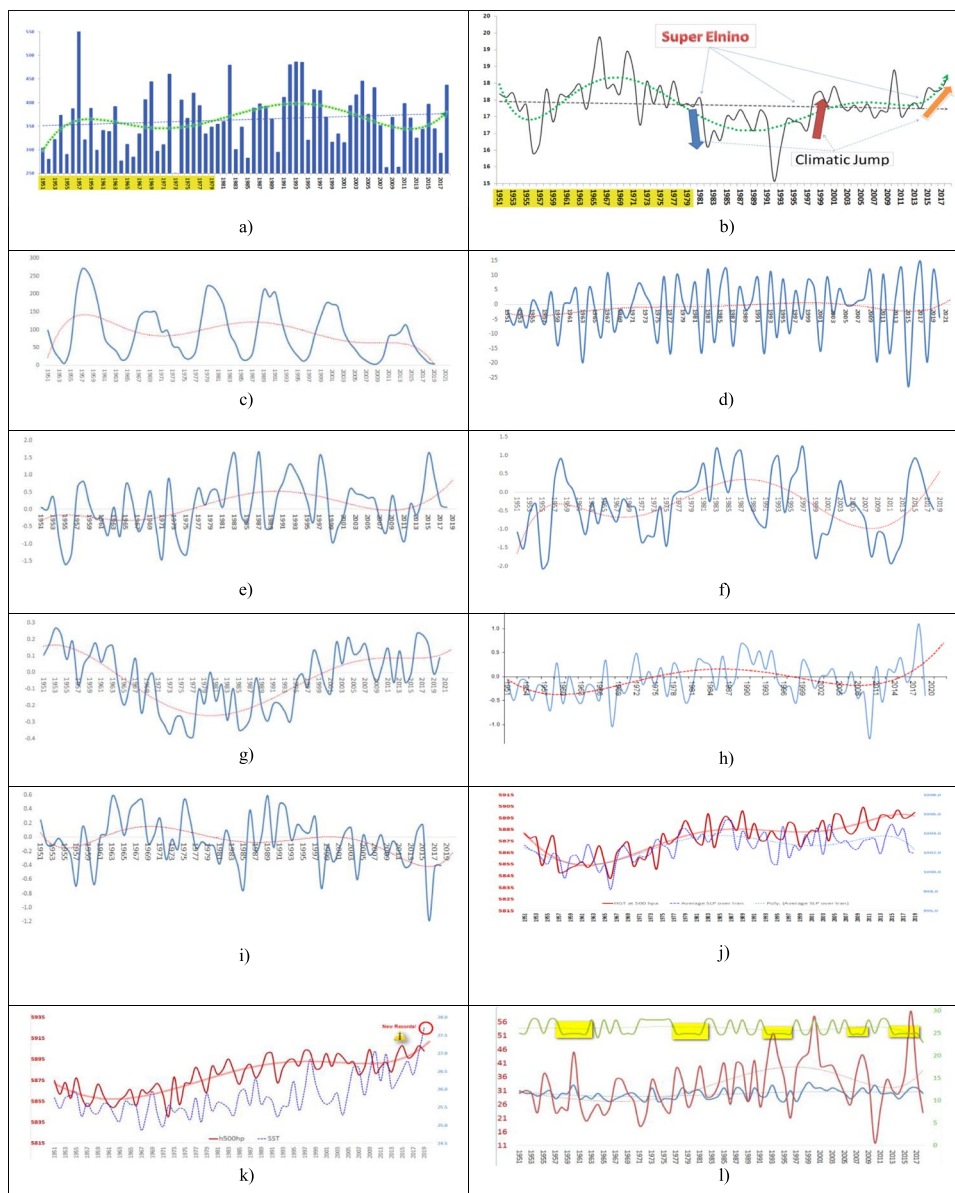


Fig. 2 The time series of some teleconnection indices, average precipitation (Iran), average temperature (Iran), and synoptic characteristic indices. Yellow color on the axis (**a** and **b**) from 1951 to 1979. Because there were limited numbers of stations compared to the continuation of the period, this section might not be highly reliable and only the general trend of temperature and precipitation was slightly informative for the interpretation. The x -axis in all diagrams corresponds to the time, and the y -axis is the representative of each mentioned index. **a** Average of The Iran's annual precipitation time series. **b** Average of the Iran's annual temperature time series according to simultaneous extreme ENSO events. **c** Average of the number of annual time series of SSPOT. **d** Average of the annual time series of QBO index. **e** Average of the annual time series of MEI index. **f** Average of the annual time series of PDO index. **g** Average of the annual time series of AMO index. **h** Average of the annual time series of NAO index. **i** Average of the annual time series of POL index. **j**

Average of the Iran's 500 hPa geopotential height (m) and Iran's plateau mean pressure (SLP in hPa); sample for July in recent years, the distance between trends of both parameters are widely shown. **k** Average of geopotential height (HGT; m) at 500 hPa over Iran and Mideast's Sea SST (c0): sample for June. Iran mean: 45 to 65° E longitude and 15 to 40° N latitude. **l** Time series of subtropical jet of Mideast at 300 hPa (October–May). Center of action: latitude (blue)/longitude (red)/speed (green, m/s); the yellow box represents the stability in wind speed. In recent years, the longitude of MJS shows more fluctuations. **m** Average of the annual time series of TNI. **n** Average of the annual time series of sun spots and Iran's average temperature (Fantastic Harmony). **o** α Average of the annual time series of Nino 3.4 and Iran's annual average precipitation (Fantastic Harmony); β average of the annual time series of Nino 3.4 and Arctic Oscillation

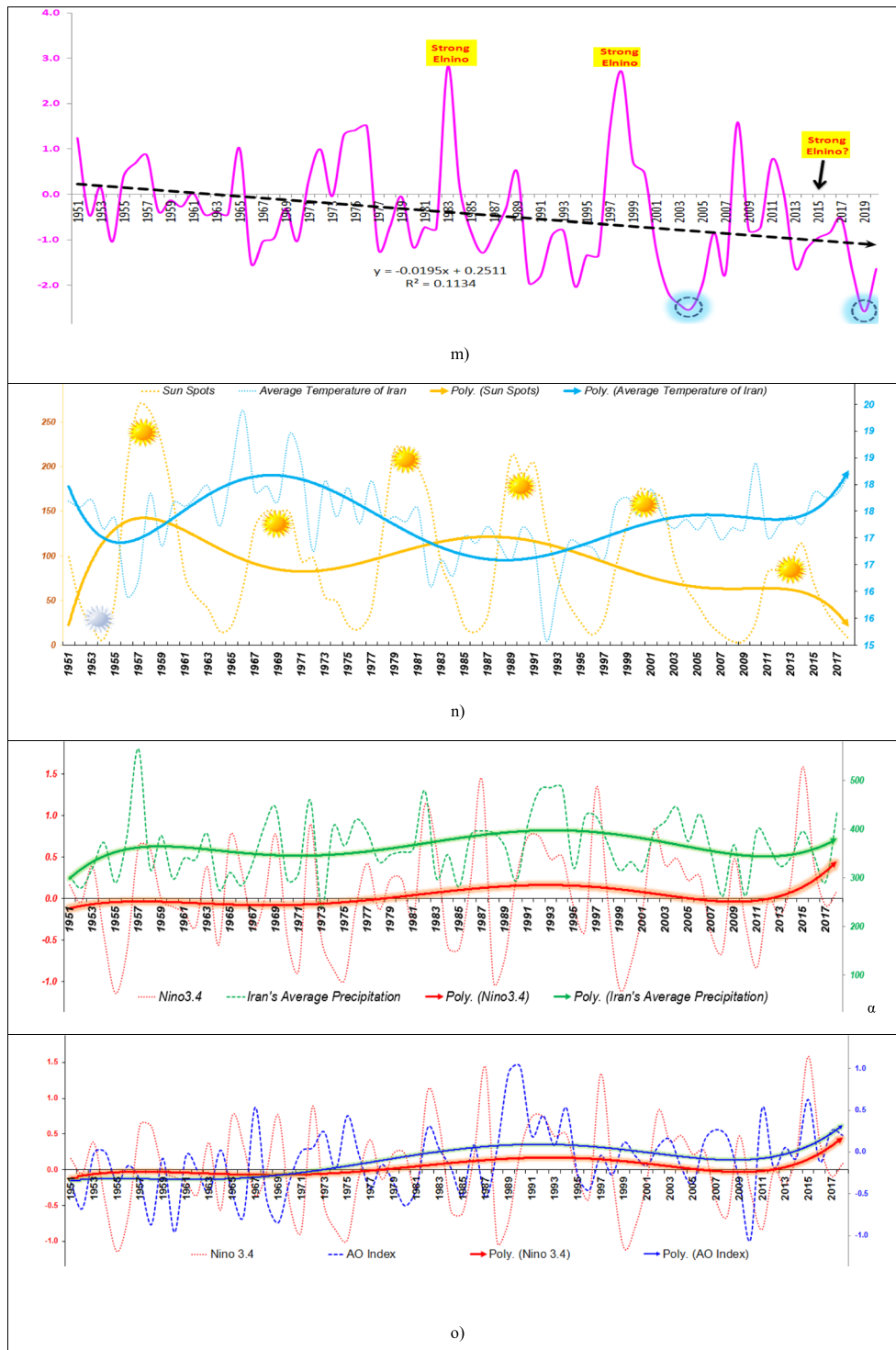


Fig. 2 (continued)

correlation coefficient was applied as weight. For example, in the ENSO method, the most similar years were 1981, 1996, 2011, 1998, and 2010 in which the average for each

station for 1 month was considered as the rainfall forecast. Most of these 5 years had similar characteristics, with dry autumns in Iran and the Middle East influenced by La Niña.

Table 3 Comparison of simulation of Iran mean temperature anomaly (°C) compared to the long term in the output of four models in Iran

Model	October	November	December	RMSE _t	Accuracy percentage of warm anomaly simulation (%)
GLB	0.73	-0.21	0.38	1.33	69
ENSO	-0.33	-0.16	1.37	1.25	47
RGN	0.12	0.15	0.57	1.34	66
ALL	0.51	-0.12	0.41	1.36	66
Accuracy	0.61	0.92	1.53	-	80

This interpretation and synoptic causation is also one of the strengths of the TSM. Recently, this time-consuming handheld compatible was written in C # and Windows Presentation Foundation (WPF) technology, a standard technology proposed by Microsoft that is widely used for programming applications. Also, a new software program (TSM) has been produced and most of the computations have been automated.

In this study, considering the effect of other forces in the atmosphere and ocean, some new indices have been added by defining the geographical box on the plotter section of NOAA site (<https://psl.noaa.gov/cgi-bin/data/timeseries/timeseries1.pl>). For example, the MDG index is actually the induction of the water temperature of the South Indian Ocean in the area of 20 to 40° south latitude and 50 to 110° east longitude. Another example is that the Mediterranean Temperature Index (MTI)² (its time series is not shown) defines two regions (boxes): the final result of the MTI using the difference between the square coverage of the Western Mediterranean from 33 to 43° north latitude and 3 to 20° east longitude and the square coverage of the Eastern Mediterranean from 32 to 37° north latitude and 20 to 34° east longitude are obtained.

Decomposition of precipitation fluctuations was not performed due to more reflection of anomalies and more weight gain of correlations and its minor effect in the final results.

In comparison with the predictions of the developing model and Climate Forecast System (CFS) experiment, another important point based on the findings of this study was that we cannot claim the efficiency of the statistical model of this research rather than other models and the purpose of this simple and single comparison was to show the ability of a simple model over complex and statistically dynamic couple models. It is because the more complexity in the model does not necessarily lead to a more accurate output. It is also emphasized that the reason for choosing the CFS model for comparison was its accessibility in the archives and monthly scale.

Even some indices that are basically non-teleconnection, such as the anomaly of the average temperature of the world, carbon dioxide, and sunspots, were added to TSMs to make it more comprehensive. Due to our broad and vast research, the interpretation of some cases and diagrams was omitted.

It is necessary to state that the present research is a combination and summary of three related topics to avoid many details. Also, some of the findings of the present study are based on a case study and the authors do not claim to be definitive for it and it is an initial effort for leading researchers to provide more in-depth theories with new research.

3 Results and discussion

3.1 Simple and visual statistical analysis

The time series of prominent teleconnection indices, some Middle East meteorological features, and the average precipitation and temperature of 36 meteorological stations were studied in Iran. The graphical representations of the results are provided in Fig. 2. Here, we represented simple, initial, and practical findings; the trend line in the time series diagram is a 6th degree polynomial (set of Fig. 2), and our objective was not to examine the significance/insignificance of the trends.

From the visual examination of Fig. 2, the following points could be highlighted:

- There was a relative simultaneity and concurrent in the fluctuation or trend in most atmospheric indices and parameters (especially in Fig. 2a, b, g, h, f).
- The average precipitation, in Iran, decreased from 1994 to 2014 and then increased until 2019. Although the period 1951 to 1980 was not referable due to the different numbers of stations, to some extent, the general trend was useful for interpretation. The year 2019 was an exceptional year. This is why it is specially modeled. In March 2019, several devastating floods occurred in the north and southwest of Iran. The amount of precipitation was so much that in Khorramabad, Gorgan, Arak, Hamedan, Bojnourd, Koohrang, Aligudarz, Sarpol-e-

² In fact, it is the zonal gradient of water surface temperature.

Zahab, Kangavar, and Islamabad-e-Qarb stations, the record of monthly precipitation was broken.

- The average temperature, in Iran, was similar to precipitation especially at year 1997 (super El Niño); it had a sharp upward trend and continued (Fig. 2b).
- The turning points and failures were observed in some indices.
- Major fluctuations in the indices occurred simultaneously or right after the extreme events of ENSO, including El Niño 1997–1998. For instance, the EA and East Atlantic–West Russian (EAWR) indices undulated startlingly after the powerful super El Niño.
- The AMO Index entered a positive phase at the end of the twentieth century and has followed the same trend since then.
- The NAO index increased in recent years. Even in the last 5 years, many record-breaking events were registered including NAO, TSA, WP, EAWR, PDO, WHWP, POL, QBO, Somalia low-level jets, the Middle East water sea temperature, zonal wind temperatures of 200 hPa in Central Pacific, Madden–Julian signal, etc. These events coincided with excessive global warming and climate changes mainly in the last 70 years.
- It seems with the declining trend of the Trans-Niño Index (TNI; data not shown), global warming, and other unknown factors; the frequency of El Niño Modoki³ has increased in recent years. In fact, the downward trend in this index indicates a change in both sides of the normalized difference between Niño 1.2 and Niño 3.4; given the warming of the Central Pacific in the last two decades, the decline is obvious.
- The multi-diagram in Fig. 2o is very useful and proves the causal effect of the oceanic–atmospheric super phenomena as the most important reason of global phenomena or other regional and hemispheric indices (e.g., NAO, AO, EAWR, PNA). The main role of teleconnection forces on the average annual rainfall of Iran was demonstrated as well.

In general, by increasing the statistical period, the fluctuations and changes in the teleconnection index time series increased and, consequently, the regression and correlation between the indices and atmospheric parameters changed. Thus, the relationships and models should be constantly evaluated, reconsidered, and updated.

³ This is a new approach when the center of Pacific Ocean is the center of action in warm or cold phase; it is named Central Pacific El Niño or La Niña (Ashok et al. 2007; Ashok and Yamagata 2009).

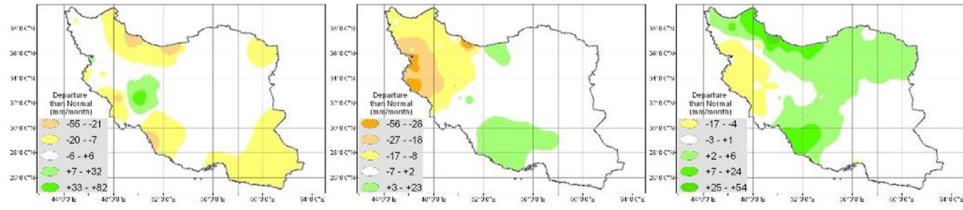
3.2 An example of a case application in seasonal forecasting

A comparison between the monthly temperature anomaly forecast of the case study in December 2017 and the observed temperature is shown in Table 3 and Figs. 3 and 4. To evaluate the four groups of indices for the October, November, and December 2017 forecasts, RGN and ENSO were more accurate and the trend and anomalies of the fall temperature (2017) were better simulated in the country. Moreover, all four models positively simulated temperature anomaly in December 2017.

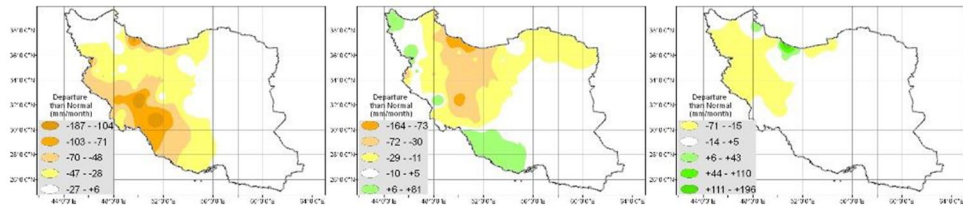
According to the map in December 2017, the increase of temperature was predicted in all synoptic stations. The RMSEs of the four groups are displayed in Table 3. The least error (1.25) happened in ENSO indices, which showed the correlation of the fall temperature with the super ENSO forcing. The most accurate and positive anomaly simulation was estimated by GLB (69%), and RGN (66%) was more appropriate in terms of trending. The best performance in simulation was obtained by RGN. By moving forward from October to December 2017, the simulation error also increased and the average error rates of the four methods in the 3 months of Fall 2017 were calculated by 1.05, 1.4, and 1.51, respectively.

The study of temperature anomalies event of Fall 2017 showed the positive anomalies in 80% of the stations; the average of the four models for this index was 62%, and to some extent, it indicated the proximity and reasonable accuracy of this simulation. According to the superior simulation in GLB, the role of global warming in the fall temperature anomalies (2017) and other unknown geophysical factors (e.g., the plate tectonic activity and increasing heavy radon gas exposure) was more than the effect of teleconnection forces. The low accuracy of ENSO model in the simulation might be the result of the negative phase of ENSO (La Niña) in the Fall 2017 and its often cooling effect on the average temperature of the Earth. From the spatial-temperature distribution point of view, the ENSO-related model was more appropriately matched to the observational records, especially in central parts of Iran (Fig. 5).

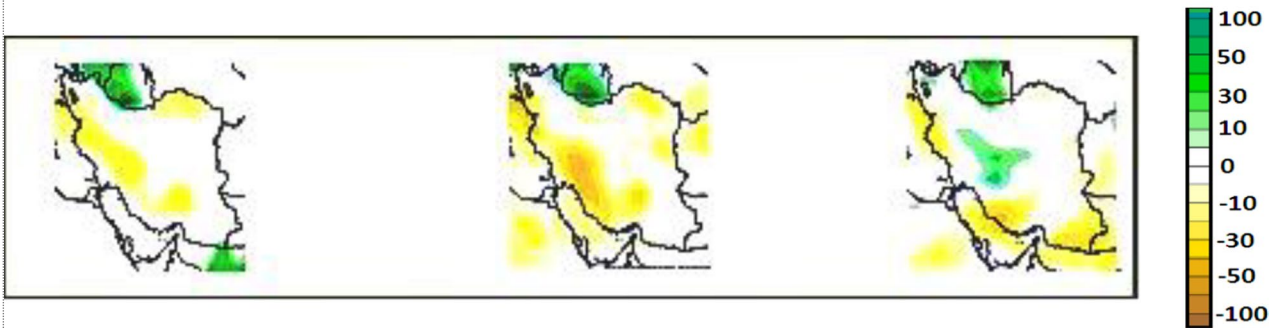
In the case of precipitation parameters, the best outputs belonged to the GLB and ALL models, especially for October and November (Table 3). It is denoted that all four models simulated and performed below the normal precipitation in October and November 2017, while RGN performed above the normal in December. However, in terms of quantity and RMSE, the observed precipitation highly differed from the estimated precipitation, especially in December. For this case study, it was a highly important finding where the relatively low impact and insignificant role of regional



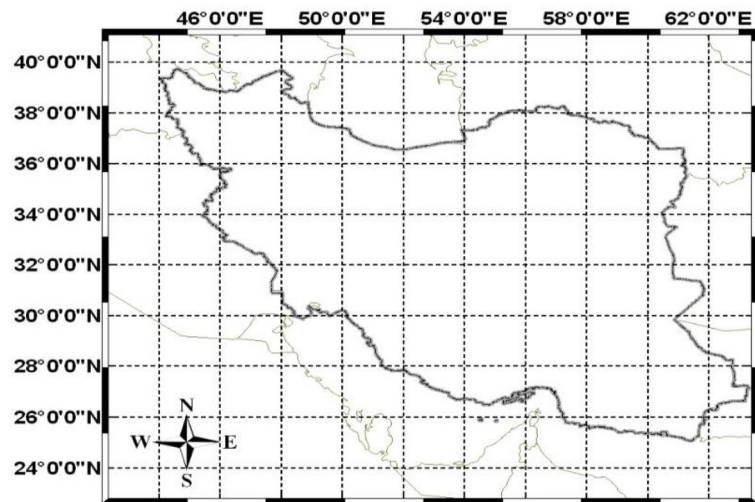
a)



b)



c)



d)

Fig. 3 **A, b** Comparison between the precipitation simulation in Fall 2017 using ALL model (per mm) and real condition. (Bottom) **c** CFSV2 area forecast model; initial condition: 18z Sep 15 2017 to 12z Sep 12 2017. Not all interpolation maps are reclassified. **d** Geographical and guide accessories of the study area of outputs. Geographical justification of the map: all the IRAN maps in this paper are (from the left (westernmost) to the right (easternmost)) from 44.1 to 63.3 eastern decimal degrees (longitude) and (from the bottom (southernmost) to the top (northernmost)) from 25.3 to 39.8 northern decimal degrees (latitude). **a** Real condition, 2017. **b** Forecasted condition (just via ALL method among the four methods of TSM), 2017. **c** CFSV2 rainfall anomaly prediction (mm), 2017. Source maps and higher quality maps were not available. **d** Geographical and guide accessories of the study area of outputs (CFSV2)

teleconnection patterns including NAO and some related indices (such as SCN and EAWR) were identified. The current study was not in agreement with many past studies that measured a higher impact of the aforementioned indices and patterns, in the region. This means that the ENSO family teleconnection patterns and common indices related to the surface temperature of the oceans were not in the strategic position to trigger extreme precipitation systems (La Niña) in Fall 2017. Therefore, regional and local patterns had little effect on frequency and strength of synoptic systems in the Middle East.

It can be stated that regional teleconnection patterns were mainly modified by the global regimes. Due to the pressure, geopotential, and small-scale nature of the most regional indices and the highly influential planetary waves, their usage created more errors in forecasting at longer distances. Another remarkable fact was that the model with a broader and wider geographical area had a higher impact and weight on the correlation analysis. It might be as a result of integrated and global indices with more contribution to the statistical correlation between atmospheric parameters and indices (Tables 3 and 4).

As shown in Fig. 3, the October 2017 precipitation forecast in the two models indicated a greater exaggeration of dry conditions in the TSM than the CFS model. For November, the spatial distribution of precipitation anomalies in the TSM was better than that in the CFS model. In December, both models were similar, but to some extent, the TSM showed better rainfall anomalies.

Comparing the outputs of the present research models with the common CFSV2 model for the precipitation simulation in Fall 2017 (Fig. 3), our models proved its robustness with higher accuracy especially for the second month (November). In addition to the record-breaking event regarding the hottest month (March) in 2018, the mentioned anomaly was well simulated by the complete model ALL (using all 52 indices) and it comparatively outperformed the CFSV2 model (Fig. 5) in a 1-month case analysis in nearly all stations.

3.3 Simple conceptual modeling of the proposed teleconnection mechanism and climatic changes

In a synoptic approach, with the use of geopotential height anomaly maps and sea level pressure in global scale with the extreme phases, the design of our method is summarized as follows.

Analyzing pressure anomaly maps, geopotential height and jet using the section of NOAA reanalyzing plotter in three extreme phases from El Niño and La Niña (to depict a more sharpened synoptic view), a simplified model with an average of the Middle East atmospheric currents was proposed. Apparently, the effects of ENSO reached to the Middle East through three mechanisms (almost simultaneous interaction) of atmospheric bridge dynamics (Fig. 6):

- A. Contraction of polar vortex in the North Pacific and its expansion in Eurasia and vice versa, where the correlation between Iceland low pressure and Aleutian is usually negative (fluctuations in NAO and NPO indices)
- B. Changing the curvature, force, and latitude of jet streams, especially in near-tropical regions, and modifying the planetary waves
- C. Changing the Walker circulation in Indian Ocean, fluctuation in air subsidence over India and the low level of Somali jet, and finally, the influences on the Indian Ocean Dipole and the humidity flux from the North Indian Ocean

Given the complex climate of the Middle East and the lack of modern and basic research, this study is also an attempt to introduce an interesting area in terms of atmosphere–ocean dynamics and the complex interaction of the Mediterranean climate, Indian monsoon, Eurasian systems including Siberian high pressure, influence of the African subtropical convergence zone by the Red Sea, and eventually, the formation of a new and semi-convergent-frontal zone in the global or regional synoptic charts (“RZCFZ”: Red Sea–Zagros convergence–frontogenesis zone, Fig. 6B). In fact, the presence of the great Zagros mountain range and its extension from near the tropical to the subtropical region (atmospheric) have a significant effect and create a southwestern slope zone of the Red Sea, perpendicular to the Zagros Mountains. This mountain range, along with the Persian Gulf–Baghdad semi-geosynclinal valley, sometimes strengthens the formation of atmospheric rivers and increases perceptible water over the Persian Gulf, Kuwait, Saudi Arabia, and Iraq even more than many tropical oceans (major in cold season from October to May). Indeed, some leading researchers are mandatory to prove this claim and the initial hypotheses.

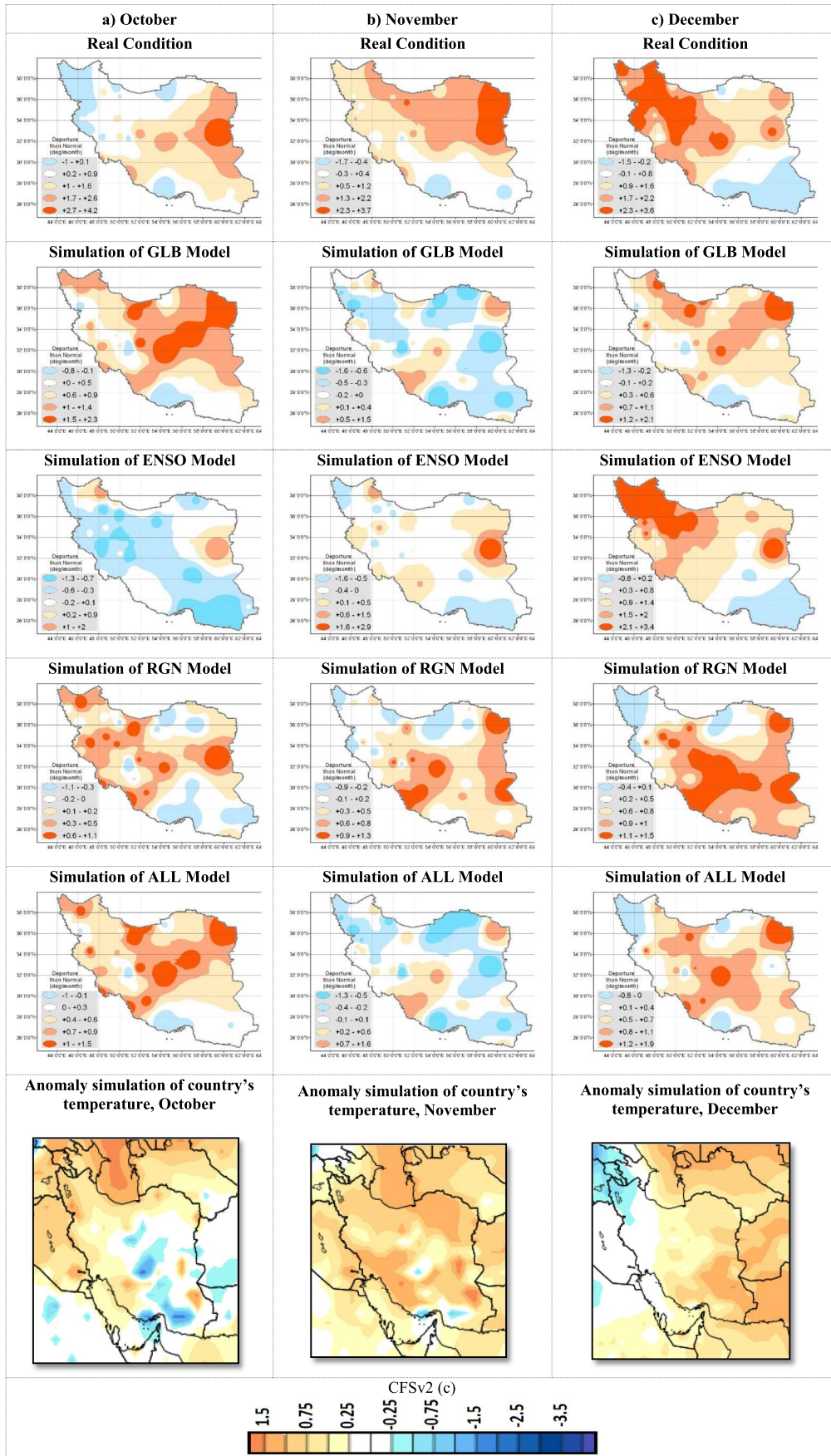


Fig. 4 Spatial comparison of temperature anomaly simulation and actual anomaly in degree Celsius (top maps: the events). The bottom is the CFSV2 model in Fall 2017 (initial condition: 18z Sep 15 2017 to 12z Sep 12 2017). Normal on the chart above means long term

several variations or changes and some initial hypotheses and theories were proposed especially based on the warm season.

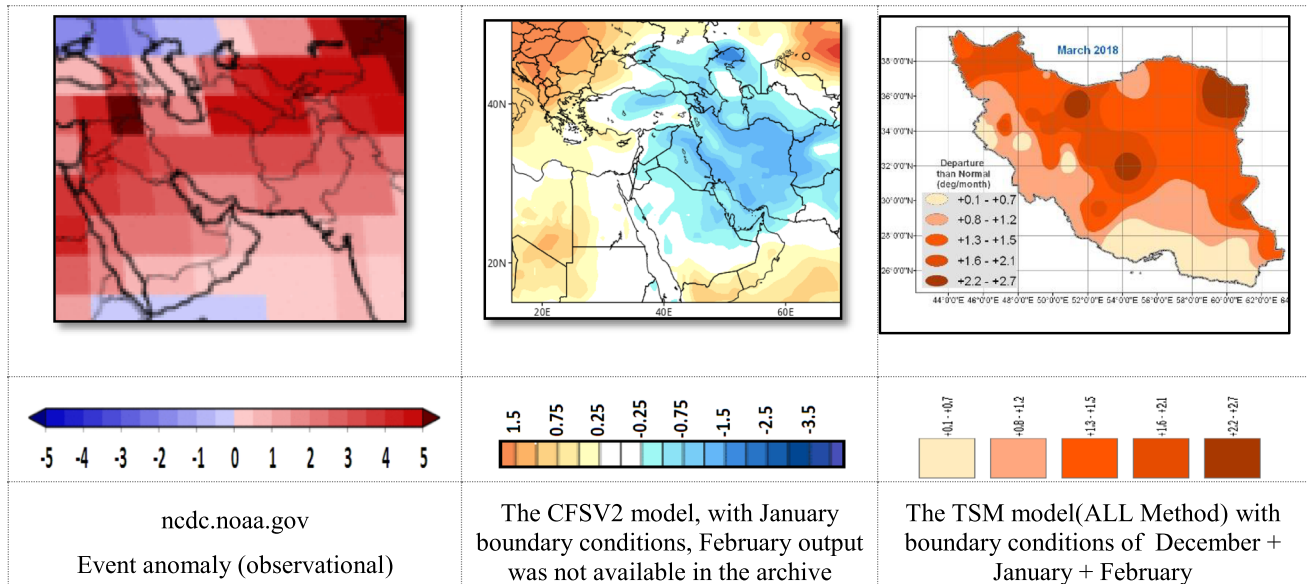


Fig. 5 Comparison of the simulations (forecast) of temperature anomaly (degree Celsius) using two models in March 2018 (left side: observational): TSM (right side) and CFSV2 model (middle) using the following initial condition: 12z Jan 25 2018 to 06z Jan 28 2018. Geographical justification of the map: all the Iran maps in this paper

are (from left (westernmost) to right (easternmost)) from 44.1 to 63.3 eastern decimal degrees (longitude) and (from bottom (southernmost) to top (northernmost)) from 25.3 to 39.8 northern decimal degrees (latitude)

Table 4 Comparisons between the average forecasted precipitation (mm) and the long term using the four models in Iran

Row	Model	December	November	October	RMSE
1	GLB	47	28.3	16.4	11.8
2	ENSO	44.1	33.4	28.7	15.5
3	RGN	55.7	42.9	15.4	19.9
4	ALL	44.6	22.3	14	13.7
Accuracy		13.3	28	17.8	–
Long term		50.5	46.3	30.9	–
RMSE		34.6	6.6	4.6	–

At the end of this section, according to the correlation of many studied patterns and trend of precipitation and temperature of the stations, especially the average temperature of the world and the issue of unbridled global warming and climate change, the increasing trend of the average temperature of water zones of the Middle East,⁴ which, in 2018–2019, reached the record of the warmest temperature with a difference of 1.1 °C more than normal, was seen. Moreover,

The average wind at the level of 850 hPa over the past decade in cold season in the North African box⁵ increased by 0.6 m/s in the long term (enhancing convergence over and around the Red Sea). However, the average wind at 850 hPa over the past decade in the warm season dropped by 1.2 m/s in less than long term (possibly weakening convergence). The aforementioned wind index had a high record in the first 4 months of 2019, and in February 2019, it reached 4 m/s more than the long term and reached the highest rate in the last 70 years (simultaneously unprecedented floods in Iran and some parts of the Middle East, despite the dry regime in the region from 1994 to 2014).

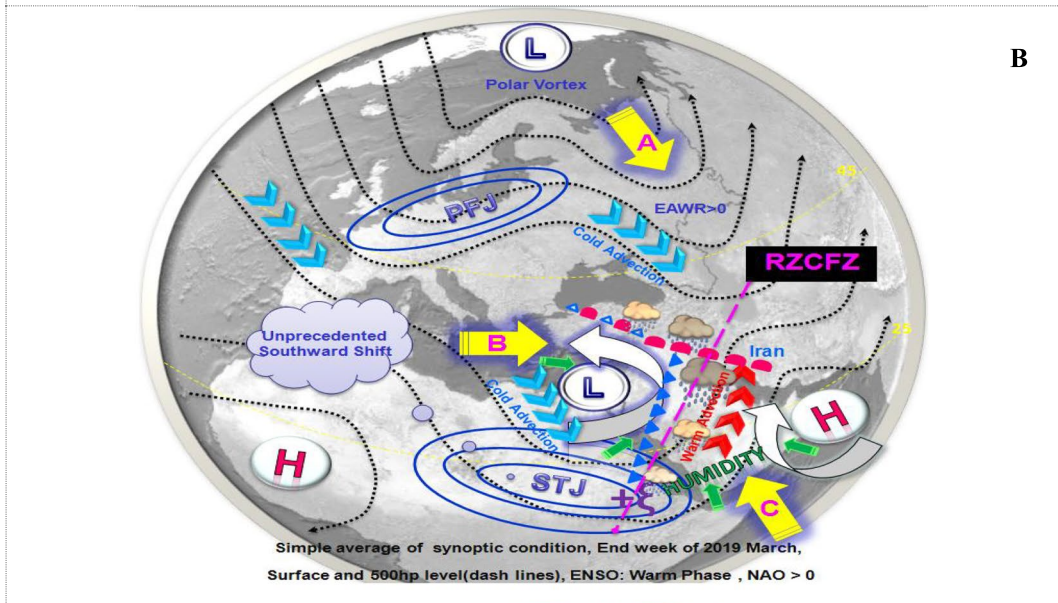
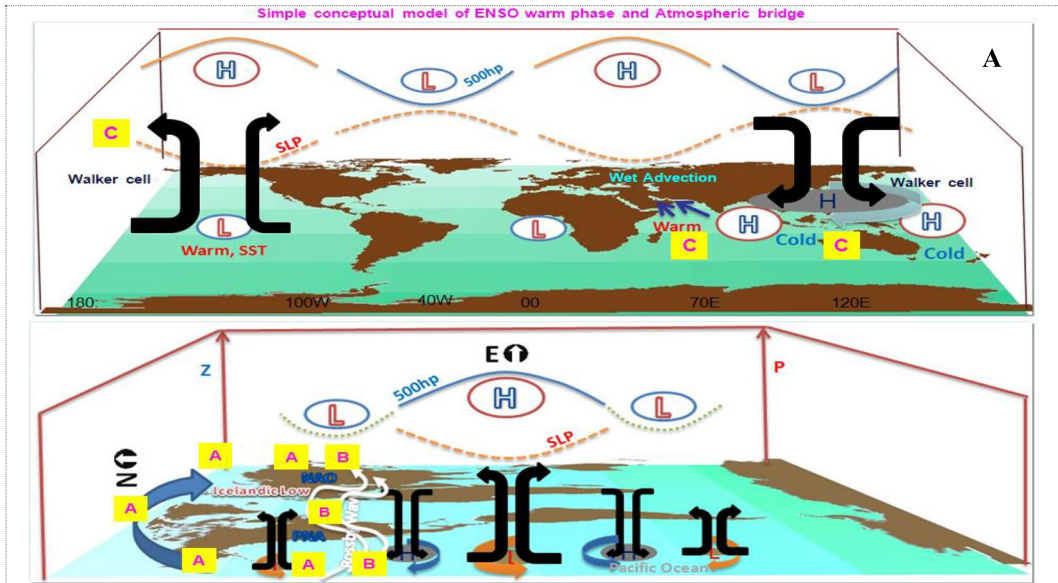
The roles of mechanisms that can change or fluctuate summer circulation patterns, especially Summer 2020, are as follows:

- Changing in the axis/center of high pressure in the upper level of Zagros
- Changing the number and amplitude of Rossby waves (incremental) and QRA mechanism
- Gradual disappearance, displacement, or weakening of the quasi-static trough in western Anatolia (summer⁶)

⁴ Mean water surface temperature of six seas of the region according to Caspian Sea, Black sea, Eastern Mediterranean, Red Sea, Persian Gulf, and North Indian Ocean.

⁵ The area average is between 10 and 22° north latitude and 10 to 35° east longitude.

⁶ Both seasonal Etesian and Shamal wind patterns have weakened over the past decade. The event is also linked to a significant reduction in dust storms in the Mesopotamia region over the past few years.



Mar-31-2019 06:12UTC
 2019 090
 Meteosat-8

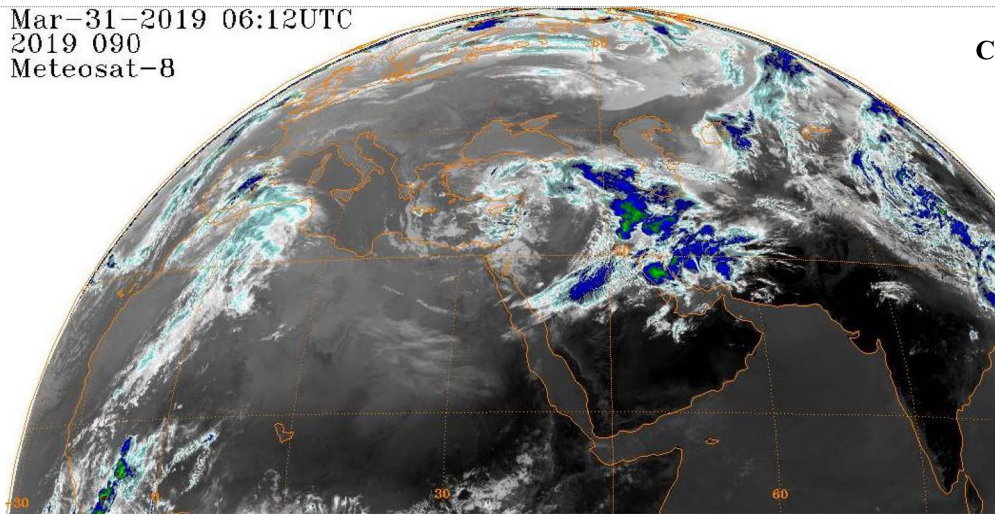


Fig. 6 The conceptual modeling of the influences of ENSO by three mechanisms of atmospheric bridge dynamics on the atmospheric general circulation and the Middle East climate (anomaly of 500 hPa height level and sea level pressure on adjacent parts and areas). **A** East–west synoptic profile (top) and north–south profile from a Western perspective (bottom). The curves on the figure show the general fluctuation of the geopotential height and air pressure in the warm phase of ENSO (in contrast to the cold phase). In fact, the mass distribution of the atmosphere changes such as the pendulum or seesaw in the pattern of the mean of the Eastern and Western Hemispheres, especially in the winter of the Northern Hemisphere and the ENSO event (using the mean pressure difference of the Western and Eastern Hemispheres, which is not shown). **B** Eurasian synoptic, profile (*STJ* subtropical jet stream, *PFJ* polar front jet stream; $+\zeta$ represents positive vorticity advection of the head or input of STJ; blue and red triangles and semicircle refer to cold and warm fronts, respectively). Latin letters also simplify the sequence and path of all three mechanisms. **C** The satellite image on March 31, 2019 (www.ncdc.noaa.gov/gibbs/html/MSG-1/IR)

- Gradual conversion of the eastern and thermal branch of Southwest Asian monsoon low-to-dynamic low pressures (especially Persian Gulf low pressure).
- Arrangement and relative attenuation of the Somalian low-level jet and northwestern shift of transient easterly waves⁷ (not shown).

It is worth noting that a significant decrease in dust storms in the warm season of the southwestern half of the country and even Iraq in recent years could be due to significant changes in summer pressure patterns in the Middle East (upper high-pressure damping⁸) and, secondarily, as a result of wet seasons in recent years.

Another significant point in the global warming⁹ and QRA mechanism was the decrease of atmospheric circulation and the increase of planetary wave number and, finally, the more creation of cutoff low pressure. In particular, simultaneous with the warm ENSO phase, it gradually leads to more powerful atmospheric rivers in the Middle East. However, the frequency of these atmospheric rivers may decrease. Also, with low frequency, during the last decade in the cold season, a tendency to penetrate and deepen more cold waves in Southwest Asia was seen.

⁷ In a way, this mechanism is the penetration of the Intertropical Convergence Zone (ITCZ) to higher latitudes. This event seems to be due to global warming and the creation of a new arrangement of pressure patterns.

⁸ The stillness and suffocation of the air is due to subsidence and deceleration of the southern strip of subtropical jet, and during the climatological period in the warm season, it blows at a level of 300 hPa over Turkey to the Caspian Sea.

⁹ In particular, pay attention to the significant increase in water temperature of the seas of Southwest Asia (Fig. 2k). These conditions in proper moisture flux patterns cause a significant increase in precipitable water and even convective available potential energy.

4 Conclusion

In recent decades, increasing human knowledge regarding the Earth climate along with extreme concern about the climate changes in the future leads to more accurately and effectively understanding of the components contributing to the climate change. One of the most significant factors which have received much attention is large-scale climate phenomena that affect the global climate change and the atmospheric cycle. Temperature and precipitation are also the most significant climate elements that affect the dispersion of other climate elements, and their fluctuations and variability are very vital especially in the fields of agriculture and water resources management with large-scale climate phenomena. In this study, the statistical analysis of teleconnection indices and modeling of the effect of ENSO forcing in Iran climate were applied. For that purpose, a preliminary statistical analysis was performed on the time series of teleconnection indices and atmospheric parameters. It indicated the existence of relative correlation and synergy in the fluctuation or trend of most atmospheric indices and parameters. On the other hand, most of the fluctuations in the indices occurred simultaneously or after the extreme events of ENSO, including El Niño in 1997–1998. For the first time in Iran, this study used the statistical correlation method between two main climate parameters and teleconnection indices to predict the monthly temperature and precipitation anomalies. First, the teleconnection indices were provided from reputable global databases and then the correlation of the teleconnection patterns was analyzed. Finally, 5 years with the highest statistical similarity with priority weighting were extracted as the representative years for the forecast. The findings revealed that up to 70% of the predictions were correct. Regarding the precipitation forecast, the best models were the GLB model using global indices followed by ALL (all teleconnection indices). The advantages of these models to similar statistical and dynamic models were the simplicity and availability of input data and high flexibility in predicting different types of atmospheric parameters. Due to the lower RMSE in the indices related to ENSO, the relationship between Iran climates (especially temperature fluctuation) and super ENSO was obvious. The analysis of the temperature anomalies in the Fall 2017 showed positive anomalies in 80% of synoptic stations. The average of all four models for temperature anomalies was equal to 66%, indicating the accuracy of the simulation. The ENSO teleconnection linkage to Iran climate emphasized on the dynamic mechanisms of the atmospheric bridge with three components of vortex contraction in the Western Hemisphere and expansion in the Eastern Hemisphere, changes in the curvature and width of STJ, and variation in the Walker cell. Unlike most relevant models with seasonal scale (e.g., International Research

Institute (IRI) of Columbia University and European Centre for Medium-Range Weather Forecasts (ECMWF)), our model used the monthly scale and the forecast could be calculated on the basis of solar month which was more practical in planning and decision making in such country, especially in the agricultural sector. This model together with other models can help the atmospheric experts and interpreters in the future. In the current research, the accuracy and reliability of the results were increased by using different models in forecasting, comparing the various models, selecting the most significant and effective teleconnection indices on the study area, and selecting a long-term statistical period with different scales (monthly and annual). The previous studies were mainly conducted by fewer teleconnection indices and models for temperature and precipitation predictions (Park and Mann 2000; Nguyen et al. 2019). Moreover, there was an agreement between the present study and another research by Chattopadhyay and Katzfey (2015) in better performance of the GLB model in precipitation prediction using teleconnection indices. It is also noteworthy that in terms of monthly and seasonal temperature modeling and forecasting in Iran, more statistical methods and artificial intelligence should be applied with acceptable results (Amini Rakan et al. 2015; Ghasemi 2017); however, less attention was paid to temperature and precipitation evaluation using teleconnection indices.

One of the main purposes of this study was to make maximum use of all available teleconnection indices for more comprehensive synoptic–statistic modeling. Three mechanisms were proposed to determine the effects of ENSO on the Iranian climate, the most important of which is through the Walker circulation atmospheric bridge and the creation of sea currents on land in the Middle East in the warm phase of ENSO. Usually at this time, the Indian Ocean Dipole Index is also positive and the humidity advection and perceptible water is strengthened. In the cold phase, the opposite happens and the northern currents intensify in the Middle East. Since the correlation between ENSO warm phase and NAO is positive, the warm phase of ENSO usually increases the frequency of NAO positively and, according to some researches (Alemzadeh et al. 2013), the positive phase of NAO enhances the cyclogenesis of the Eastern Mediterranean, so we concluded that ENSO almost controls the indices under its regional influence, including NAO, Iran's rainy climate.

As a final result of this research especially by visual inspection of time series, we observed the reflection of main climatic forces such as ENSO in the time series of precipitation and average temperature of Iran.

Another point is the change of climate regime in the Middle East and the planet after each super El Niño event. For instance, after 1982, a relatively humid cold period

prevailed in Iran. After El Niño in 1997, a warm and dry period prevailed, and after El Niño in 2015, a relatively warm and humid period prevailed. However, the state of the 2015 El Niño event changed due to the dramatic negative trend in the TNI compared to other super El Niño events. In fact, “the ENSO phenomenon is the beating heart of the Global Teleconnection System.” Also in this research, the RZCFZ convergence region in the Middle East was introduced for the first time. This convergence zone was strongly enhanced in the warm phases of ENSO (for example, in March 2019).

In this work, for the first time, the time series of hyper-linked indicators related to the atmospheric features of the Middle East and Iran are presented in a simple and clear frame, so the diagrams shown in this article are very useful for interpretation and self-pacing, and even the turning point of 1997, when the most powerful El Niño occurred, followed by patterns of pressure and trend change, at least in the Middle East, is less commonly seen in similar works.

Also under the influence of global warming and especially synchronization with an El Niño event, stronger atmospheric rivers might occur in the Middle East and Southwest Asia.

Although this hypothesis is likely to be a challenge in regional circulation, it is a small step in further understanding the interaction among the centers of action in this region and some hypotheses were presented for further research on changing patterns of synoptic aspects in Iran and the Middle East.

In the present study, an attempt has been made to use very simple but practical methods and the results can help in weather forecasting, climate change detection, and conceptual–educational synoptically modeling, something that has been less seen in most recent researches, including and just for example Asakareh and Ashrafi (2012), Atif et al. (2020), Park and Mann (2000), and Nguyen et al. (2019). In the end, the authors of this article emphasize again the simplicity of the method; complex methods do not necessarily response better; they are even sometimes misleading.

Acknowledgements This research would not have been possible without having the kind link data from reputable global centers, in particular NOAA, Australian Meteorological Agency, and KNMI Climate Explorer (climexp.knmi.nl).

Author contribution M. A., M. K., S. S., and S. A. H. conceived of the presented idea and developed the theory and performed the computations. M. K. and S. S. verified the analytical methods. S. A. H. and S. S. investigated and supervised the findings of this work. Y. K., S. H., G. M. M., V. S., I. B., and Z. Y. encouraged and developed the theoretical formalism. All authors discussed the results and contributed to the final manuscript.

Data availability The data used in this paper have been prepared by the National Oceanic and Atmospheric Administration (NOAA), Bureau of Meteorology (BOM), Japan Meteorological Agency (JMA), and KNMI Climate Explorer (climexp.knmi.nl).

Code availability Not applicable.

Declarations

Ethics approval and consent to participate Not applicable, because this article does not contain any studies with human or animal subjects. The data of this research were not prepared through a questionnaire.

Consent for publication The authors of the article make sure that everyone agrees to submit the article and is aware of the submission.

Conflict of interest The authors declare no competing interests.

References

- Ahmadi M, Saadoun S, Hosseini SA, Poorantiyosh H, Bayat A (2019) Iran's precipitation analysis using synoptic modeling of major teleconnection forces (MTF). *Dyn Atmos Oceans* 85:41–56
- Alemzadeh S, Ahmadi-Givi F, Mohebalhojeh A, Nasr-Isfahani M (2013) Statistical-dynamical analysis of the mutual effects of NAO and MJO. *Iranian J Geophysics* 7(4):64–80
- Amini Rakan A, Haghighatjou P, Khalili K, Behmanesh J (2015) Evaluation the performance of genetic programming in modeling mean monthly temperature in different climates of Iran. *J Agric Meteorol* 3(1):13–24
- Asakareh H, Ashrafi S (2012) Modeling the number of days of annual precipitation based on relative humidity and annual temperature “a case study of Zanjan Station.” *Scie- Res Quarterly Geograph Data (SEPEHR)* 20(80):13–17
- Atif RM, Almazroui M, Saeed S, Abid MA, Islam MN, Ismail M (2020) Extreme precipitation events over Saudi Arabia during the wet season and their associated teleconnections. *Atmos Res* 231:104655. <https://doi.org/10.1016/j.atmosres.2019.104655>
- Bridgman A, Oliver EJ (2006) *The global climate system patterns, processes, and teleconnection*. Cambridge Univ Press. <https://doi.org/10.1017/CBO9780511817984>
- Chace TN, Pielke SRR, Avissar R (2006) Teleconnection in the Earth system, encyclopedia of hydrological sciences. Edited by M Anderson. John Wiley & Sons, Ltd Global Hydrology. <https://doi.org/10.1002/0470848944.hsa190>
- Charabi Y (2009) Arabian summer monsoon variability: teleconexion to ENSO and IOD. *Atmos Res* 9(1):105–117
- Chattopadhyay M, Katzfey J (2015) Simulating the climate of South Pacific islands using a high resolution model. *Int J Climatol* 35:1157–1171
- Darand M, Pazhoh F (2019) Synoptic analysis of sea level pressure patterns and vertically integrated moisture flux convergence VIMFC during the occurrence of durable and pervasive rainfall in Iran. *Dyn Atmos Oceans* 86:10–17
- Dayan U, Nissen K, Ulbrich U (2016) Atmospheric conditions inducing extreme precipitation over the Eastern and Western Mediterranean. *Nat Hazards Earth Syst Sci* 15:525–544
- Ding Q, Wang B (2005) Circumglobal teleconnection in the Northern Hemisphere summer. *American Meteorological Society. J Clim* 18(17):3483–3505
- Gerlitz L, Vorogushyn S, Apel H, Gafurov A, Unger-Shayesteh K, Merz B (2016) A statistically based seasonal precipitation forecast model with automatic predictor selection and its application to Central and South Asia. *Hydrol Earth Syst Sci* 20:4605–4623
- Ghasemi AR (2017) Modeling feasibility and prediction of minimum and maximum temperature in Iran by Bettitt and Holt-Winters methods. *Res Geograph Sci* 16(43):7–24
- Goudarzi M, Ahmadi H, Hosseini SA (2017) Examination of relationship between teleconnection indexes on temperature and precipitation components (case study: Karaj synoptic stations). *Iranian J Ecohydrol* 4(3):641–651
- Helali J, Salimi S, Lotfi M, Hosseini SA, Bayat A, Ahmadi M, Naderizarneh S (2020) Investigation of the effect of large-scale atmospheric signals at different time lags on the autumn precipitation of Iran's watersheds. *Arab J Geosci* 13:932. <https://doi.org/10.1007/s12517-020-05840-7>
- Helali J, Asaadi S, Jafarie T, Habibi M, Salimi S, Momenpour SE, Shahmoradi S, Hosseini SA, Hessari B, Saeidi V (2022) Drought monitoring and its effects on vegetation and water extent changes using remote sensing data in Urmia Lake watershed, Iran. *Journal of Water and Climate Change*. <https://doi.org/10.2166/wcc.2022.460>
- Honar T, Niko MR, Zand Parsa S, Siasar H (2016) Forecasts based on the standardized precipitation index and Markov drought to crops in the plains of Sistan 2nd International Conference on Agricultural Engineering and Natural Resources. Tehran, Iran
- Klein SA, Brian JS, Ngar-Cheung L (1999) Remote sea surface variation during ENSO; evidence for a tropical atmospheric bridge. *J Clim* 12(4):917–932
- Mohammadpour Penchah, M., Taghizadeh, H. (2016) Time series analysis and forecasting of monthly rainfall and temperature using ARIMA models case study, Bandar Abbas. 17th Iranian Geophysical Conference. Tehran, Iran
- Naveendrakumar G, Vithanage M, Kwon HH, Chandrasekara SSK, Iqbal MCM, Pathmarajah S, Fernando WCDK, Obeysekera J (2019) South Asian perspective on temperature and rainfall extremes: a review. *Atmos Res* 225:110–120
- Nguyen TV, Mai KV, Nguyen PNB, Juang HMH, Nguyen DV (2019) Evaluation of summer monsoon climate predictions over the Indochina Peninsula using regional spectral model. *Weather Clim Extremes* 23:100195
- Park J, Mann ME (2000) Interannual temperature events and shifts in global temperature: a “multiwavelet” correlation approach. *Earth Interact* 4:1–36
- Rezaie M, Memarian M (2014) Use of rainfall time series and large climate indices to predict drought with CANFIS network. The second conference on watershed science and engineering. Birjand, Iran
- Salimi S, Balyani S, Hosseini SA, Momenpour SA (2018) The prediction of spatial and temporal distribution of precipitation regime in Iran: the case of Fars Province. *Model Earth Syst Environ* 4:565–577
- Schwing FB, Mendelssohn R, Bograd SJ, Overland JE, Wang M, Ito S (2009) Climate change, teleconnection patterns, and regional processes forcing marine populations in the Pacific. *J Mar Syst* 79(3–4):245–257
- Shifteh B, Ezani A, Tabari H (2012) Spatiotemporal trends and change point of precipitation in Iran. *Atmos Res* 113:1–12
- Shiravand H, Hosseini SA (2020) A new evaluation of the influence of climate change on Zagros oak forest dieback in Iran. *Theor Appl Climatol* 141:685–697
- Yari D, Nahtaji M, Khaledian A (2014) Monthly precipitation forecast at Saghez synoptic station using artificial neural network. The first national conference on water, man and land. Zabol, Iran

Publisher's note Springer Nature remains neutral with regard to jurisdictional claims in published maps and institutional affiliations.